ACS APPLIED ELECTRONIC MATERIALS

pubs.acs.org/acsaelm Article

Nanowire-Shaped MoS_2@MoO_3 Nanocomposites as a Hole Injection Layer for Quantum Dot Light-Emitting Diodes

Nasim Bastami, Ehsan Soheyli,* Ayşenur Arslan, Reza Sahraei,* Ahmet Faruk Yazici, and Evren Mutlugun*

Cite This: *ACS Appl. Electron. Mater.* 2022, 4, 3849−3859 Read Online

ACCESS | Metrics & More | Article Recommendations | Supporting Information

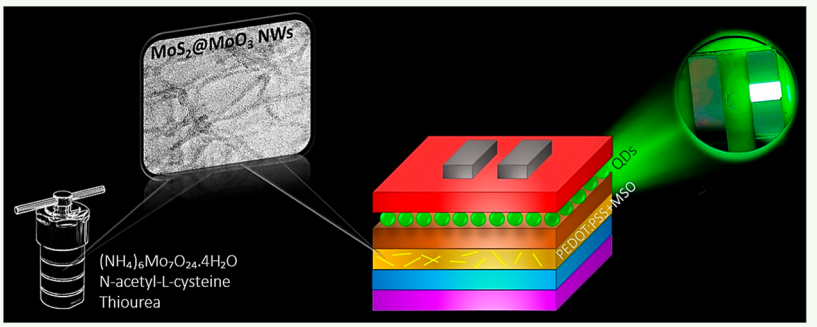

ABSTRACT: Molybdenum disulfides and molybdenum trioxides are structures that possess the potential to work as efficient charge transport layers in optoelectronic devices. In the present study, as opposed to the existing Mo-based nanostructures in flake, sheet, or spherical forms, an extremely simple and low-cost hydrothermal method is used to prepare nanowires (NWs) of MoS_2@MoO_3 (MSO) composites. The synthesis method includes several advantages including easy handling and processing of inexpensive precursors to reach stable MSO NWs without the need for an oxygen-free medium, which would facilitate the possibility of mass production of these nanostructures. The structural analysis confirmed the formation of MSO nanocomposites with different Mo valence states, as well as NWs of average length and diameter of 70 nm and 5 nm, respectively. In order to demonstrate their potential for optoelectronic applications, MSO NWs were blended into hole injection layers (HILs) in quantum dot-based light-emitting diodes (QLEDs). Electroluminescence measurements show a substantial enhancement in both luminance (from 44,330 to 68,630 cd.m^{-2}) and external quantum efficiency (from 1.6 to 2.3%), based on the increase in the ratio of MSO NWs from 3 to 10%. Interestingly, the addition of 10% volume of MSO NWs resulted in a remarkably smoother HIL with improved current efficiency and stability in green-emitting QLEDs. The simplicity and cost-effective features of the synthesis method along with outstanding favorable morphology demonstrated their ability to enhance the QLED performance and mark them as promising agents for optoelectronics.

KEYWORDS: *MoS_2@MoO_3, nanowire, nanocomposite, hole-transport layer, roughness, electroluminescence*

INTRODUCTION

Nowadays, one of the most active fields in science and technology is related to optoelectronic devices based on luminescent colloidal semiconductor nanocrystals (NCs) to foster their optoelectronic performance.[1] Among various technologies, the fabrication of quantum dot-based light-emitting diodes (QLEDs) and light-display panels is the most prominent application due to their impact on either the basic science behind the physical concepts of optoelectronics or the commercialization of optoelectronics.[2] In this regard, different approaches have been considered to attain devices with improved performances, including utilization of different materials as the emissive layer, design of interface among subsequent layers with proper architecture, and modification of charge transport layers. Without underestimating, the great importance of the two first routes, using a new material for the transport layer, has recently captured the attraction of researchers.[3]

Generally, poly(3,4-ethylenedioxythiophene)/poly(styrene sulfonate) (PEDOT/PSS) layer is used as a hole transport layer (HTL), and ZnO-based nanoparticles are used as an effective electron transport layer in QLEDs.[4] While PEDOT/PSS is the most popular agent which works simultaneously as a HTL and a hole injection layer (HIL) in industry, low

Received: April 14, 2022
Accepted: July 11, 2022
Published: August 1, 2022

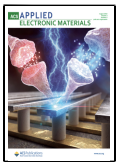

conductivity and stability problems attributed to low acidity (pH = 1) and the hygroscopic nature of PSS attack the efficiency and long-term stability of the QLED device.[5] Therefore, introducing new materials, developing the existing materials, or carrying out special treatment processes can be considered to enhance the hole injection/transport capability of PEDOT/PSS. Various reports have been dedicated to following up on this demanding progress. Khasim et al. considerably enhanced the conductivity of a PEDOT/PSS film from 1.5 to 1826 S.cm^{-1} via *N*,*N*-dimethylformamide doping and camphor sulfonic acid post-treatment.[6] They showed that the new thin layer preserves the high transparency of the polyethylene terephthalate (PET) substrate while it is still stable with improved electrochemical properties. Song et al. also used an extra graphene oxide layer to decrease the interfacial barrier energy between the anode and PEDOT/PSS layers, with a reduction in turn-on voltage from 8.35 to 5.35 V.[7] In another study, researchers have used exfoliated MoS_2 flakes and a formulated ink as an alternative to PEDOT/PSS in LED devices based on CdSe/ZnCdS NCs.[8] They confirmed that the measured external quantum efficiency (EQE) is comparable to the control device with the PEDOT/PSS layer. Also, the designed QLED preserved more than 50% of the initial record for a longtime (100 days) storage in a common air atmosphere. Recently, some reports have also suggested doping inorganic salts like NaCl or NiO nanoparticles into PEDOT/PSS HTLs in QLEDs.[9,10]

Among such strategies, employing transition-metal dichalcogenides has attracted the attention of the research community. The most promising one is molybdenum-based structures that already demonstrated that they are more active than other materials to promote the charge transport in optoelectronic devices.[11,12] Using MoO_3 or MoS_2 nanostructures as a separate layer or additive in the PEDOT/PSS layer has been reported in various LEDs with different light-emitting layers such as perovskite NCs,[13] Cd-based QDs,[14] carbon dots,[15] InP-based QDs,[16] and even organic molecules.[17] Nonetheless, in most cases, minimal attention has been dedicated to the synthesis of such MoO_3 or MoS_2 nanoparticles. Sorrentino et al. have used MoS_2 nanosheets to show that the addition of this water-soluble and highly concentrated solvent to the PEDOT: PSS layer can boost the efficiency of Cd-based QLED while improving the stability up to 41 days.[18] However, they have used bulk MoS_2 powders to prepare their nanocomposites. Singh et al. recently reported a synthesis approach for the preparation of MoS_2/MoO_3 nanocomposite as a gas-sensing agent.[19] Although their method is straightforward, it needs multiple steps with a longtime reaction process. On the other hand, as MoO_3 is a p-type semiconductor, it can facilitate the mobility of holes via an increase in the concentration of carriers as well as a reduction in the density of traps.[16] From the morphological perspective, almost all reports in this field reported nanosheets/multiple layers or QDs of MoO_3 or MoS_2 structures for the fabrication of LEDs.[17,20,21] Indeed, there are only a few reports that assert synthesizing such nanostructures in NW shape but in much bigger sizes relative to what was observed in the present study.[22−24] Guo et al. designed a two-step-synthesized MoS_2@MoO_3 core−shell NW with a diameter of 250 ± 30 nm and broad-band absorption as well as good interfacial engineering for stable H_2 evolution characteristics (841.4 μmol.h^{-1}.g^{-1}).[23] In another report, a direct anion-exchange reaction of the MoO_3 NWs was employed to produce a one-dimensional hierarchical core−shell MoO_3@MoS_2 structure containing two-dimensional ultrathin MoS_2 nanosheets.[24]

In the present study, novel NW-shaped MoS_2@MoO_3 (MSO) composites have been prepared via a facile hydrothermal method in a relatively short time and at temperatures below 200 °C. A well-known thiol capping agent was used to control the growth rate and morphology of nanocomposites, as well as to have the role of a second sulfur precursor via its −SH functional groups. The present MSO NWs showed an unusual ultra-narrow and strong emission in the green region of the visible spectrum, under UV excitation. Having a simultaneous intrinsic potential for promoting the carrier transfer along with their NW shape which is desired for transport purposes makes them excellent candidates in optoelectronic and photovoltaic applications. To support this assertion, the as-prepared MSO NWs were used in the fabrication of QLEDs with improved results in luminance and EQE. The performance-enhancing property of NWs was investigated by adding them to the PEDOT/PSS HIL in the QLED device structure. Device performance measurements were performed by adding MSO nanocomposites to the PEDOT/PSS solution. The simplicity of the synthesis and use of low-cost precursors, along with demonstrated improvements in the efficiency of CdSe/ZnS-based QLEDs, confirm the vitality of the present unique-morphology MSO nanocomposites for future optoelectronic and photovoltaic applications.

EXPERIMENTAL SECTION

Materials. Ammonium heptamolybdate ($(NH_4)_6Mo_7O_{24}.4H_2O$, ≥99%), *N*-acetyl-L-cysteine ($C_5H_9NO_3S$, ≥99%), thiourea (CH_4N_2S, ≥99%), sodium hydroxide (NaOH, ≥99%), hydrochloric acid (HCl), and acetone (≥99%) were purchased from Merck company. 1-Octadecene (ODE, 90%), acetone (99.5% from Tekkim), aluminum (≥99.999%), cadmium oxide (CdO, 99.99%), chlorobenzene (anhydrous, 99.8%), dimethyl sulfoxide (DMSO, from Merck), ethanol (≥99.9%), methanol (≥99.8% from Tekkim), n-hexane (≥98% from Tekkim), octane (anhydrous, ≥99%), oleic acid (OA, 90%), poly(3,4-ethylenedioxythiophene) polystyrene sulfonate (PEDOT/PSS, from Ossila), selenium (Se, 99.99%), sulfur (S, 99.98%), poly[(9,9-dioctylfluorenyl-2,7-diyl)-co-(4,4'-(*N*-(4-*sec*-butylphenyl) diphenylamine)] (TFB, Mw > 30,000 from Lumtec), tetramethylammonium hydroxide pentahydrate (TMAH, ≥97%), trioctylphosphine (TOP, 97%), and zinc acetate dihydrate (Zn(OAc).2H_2O, 99.999%) were utilized. All chemicals were purchased from Sigma-Aldrich unless otherwise reported and used without further purification. Deionized (DI) water was also used throughout the work.

Synthesis of MSO NWs. A hydrothermal method was used for the preparation of MSO NWs. Typically, 0.37 mmol Mo precursor, 0.9 mmol NAC, and 0.74 mmol thiourea (TU) were added to 40 mL of DI water. Then, the mixture was vigorously stirred at 0−4 °C (using an ice bath) in a three-necked round-bottom flask for 1 h to completely dissolve the powders (it should be noted that there is no necessity to use a condenser). After that, the pH of the solution was fixed at the desired amount using a 1 M solution of NaOH or 0.1 M solution of HCl (2, 3.7, 5.5, and 8). The final solution was poured inside a Teflon-lined stainless steel 100 mL autoclave reactor. Next, the reactor was transferred to an oven at a chosen temperature (140, 165, and 185 °C) and heated for a particular time duration (2, 4, and 6 h). After the completion of the reaction, the autoclave was taken outside to reach room temperature. The obtained solution was filtered using 0.22 μm filters; then, 2.5 mL of the solution was diluted with 2.5 mL of DI water and used for optical measurements. Besides, to precipitate the NWs, the as-prepared solutions were centrifuged at 5000 rpm for 15 min and then dried at 50 °C overnight. It should be noted that the precursor amounts mentioned above is typical, and it

https://doi.org/10.1021/acsaelm.2c00485
ACS Appl. Electron. Mater. 2022, 4, 3849−3859

Scheme 1. Schematic Illustration of the Synthesis Procedure for MSO NWs

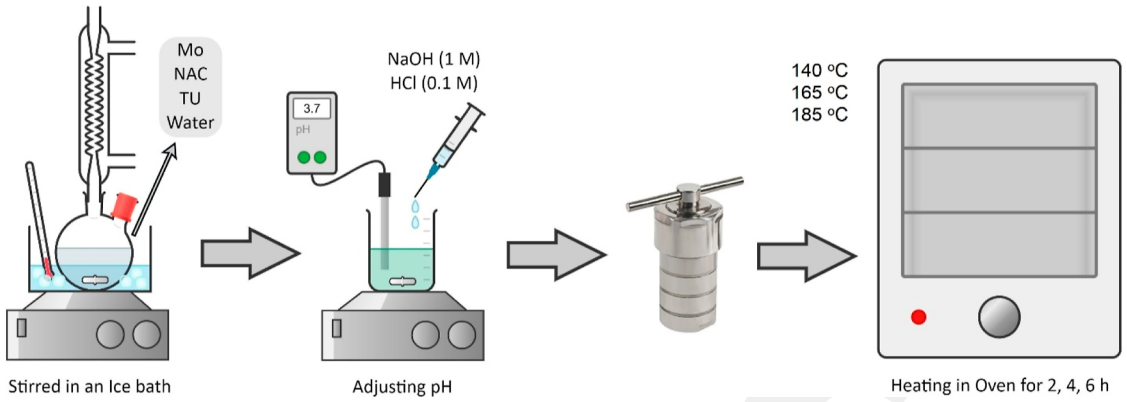

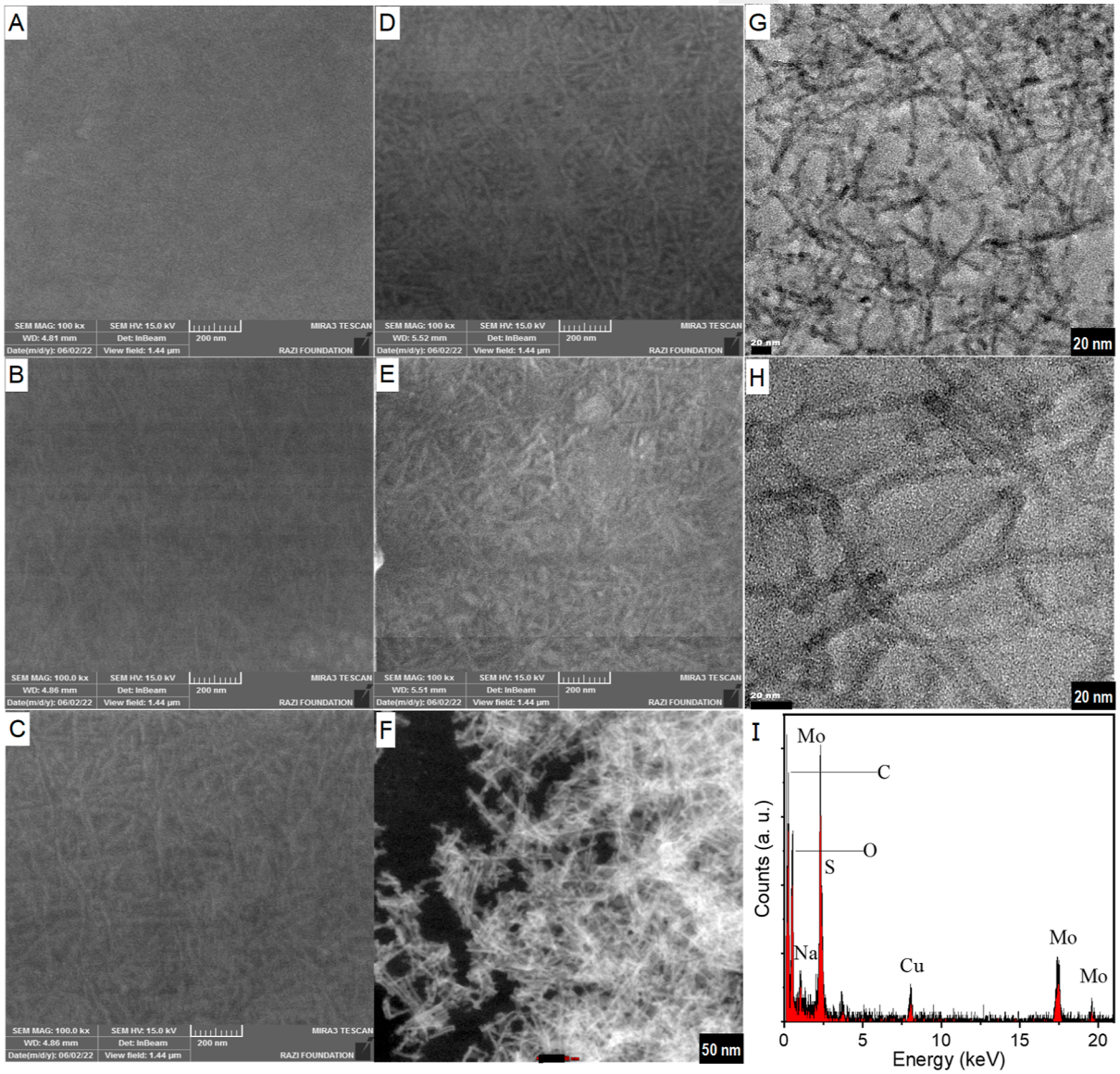

Figure 1. (A–E) FESEM images of the nanocomposites prepared at different reaction times of 1, 2, 3, 4, and 6 h, respectively (magnification = 200 nm). (F) HAADF-STEM (magnification = 50 nm), (G,H) TEM images (magnification = 20 nm) and (I) EDX profile obtained from HAADF-STEM for optimized MSO NWs prepared at 4 h.

was also optimized. Scheme 1 summarizes the synthesis recipe used in this present study.

Synthesis of QDs. Green-emitting CdSe/ZnS QDs were synthesized according to the previously reported method.[25] Typically, 1.2 mmol CdO, 16 mmol $Zn(OAc).2H_2O$, and 20 mL of OA were

https://doi.org/10.1021/acsaelm.2c00485
ACS Appl. Electron. Mater. 2022, 4, 3849–3859

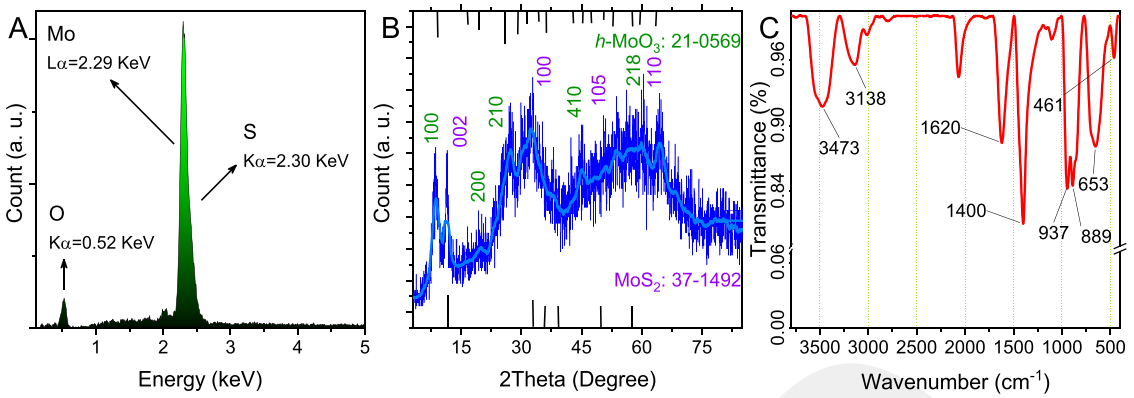

Figure 2. (A) SEM-based EDX profile, (B) XRD pattern, and (C) FT-IR spectrum of MSO NWs prepared at 185 °C for 4 h.

placed in a round-bottom flask. The mixture was heated up to 130 °C under vacuum and kept at this temperature down to 20 mTorr pressure. Then, the solution was cooled down to 70 °C, and 60 mL of ODE was added. The temperature was elevated to 300 °C under a nitrogen atmosphere. 1.2 mmol Se and 12 mmol S were dissolved in 8 mL of TOP inside an argon-filled glovebox and injected swiftly to the reaction at 300 °C. The flask was cooled down to room temperature after 10 min. QD purification was performed via centrifugation in excess acetone and methanol at 5000 rpm for 10 min. QDs redispersed in n-hexane, and precipitation repeated. Finally, QDs redispersed in octane with 20 mg/mL concentration and were used in device fabrication.

ZnO Synthesis. Zinc oxide nanoparticles were synthesized according to a modified version of the previously reported method.[26] 3 mmol $Zn(OAc).2H_2O$ was dissolved in 30 mL of DMSO. Separately, 5 mmol TMAH was dissolved in 10 mL of ethanol. Then, the latter solution was added dropwise to the former solution with constant stirring. At the end of 1 h, the reaction was completed. The crude solution was precipitated with excess acetone at 5000 rpm for 5 min. After redispersing in ethanol, second precipitation was carried out with excess acetone and hexane at 5000 rpm for 10 min. Finally, it was redispersed in ethanol with 20 mg/mL concentration and used in device fabrication.

Device Fabrication. For device fabrication, indium tin oxide-coated glass substrates with 20 Ω/sq sheet resistance were purchased from Ossila. Initially, for the cleaning step, the substrates were sonicated in 0.1% volume fraction of Hellmanex III/boiled DI water, boiled DI water, and isopropyl alcohol for 7 min each, respectively. The substrates dried with nitrogen gas were treated in a plasma-cleaning device. The PEDOT:PSS (HIL, Al 4083) solution was sonicated for 10 min. After filtrating with a 0.45 μm PTFE filter, PEDOT:PSS mixtures were prepared by adding MOS in volume ratios of 3, 7, and 10%. As soon as the plasma cleaning was completed, the PEDOT:PSS/MOS mixtures were spin-coated on the substrates at 4500 rpm for 60 s and baked in air at 150 °C for 15 min. Then, all substrates were transferred to an argon-filled glovebox and remained inside throughout fabrication. TFB solution (8 mg/mL, chlorobenzene) was coated on the substrates as a HTL at 3000 rpm for 60 s and baked at 150 °C for 30 min. EML was spin-deposited on the TFB layer as 20 mg/mL QD solution at 1500 rpm for 30 s and annealed at 60 °C for 15 min. Subsequently, the zinc oxide (ZnO, ETL) solution was spin-coated at 2000 rpm for 60 s and baked at 80 °C for 30 min. For the cathode layer, 100 nm aluminum was coated by thermal evaporation at a high vacuum (10^{-6} Torr). Finally, the devices were encapsulated with UV-curable epoxy and ≈0.5 mm thick coverslips.

Instruments. A digital scale of Sartorius AG Co.-A5002 with an accuracy of 0.01 mg was used to measure the mass of raw materials. The XRD, EDS, XPS, FT-IR, FESEM, TEM, HAADF-STEM, AFM, photoluminescence excitation/emission (PLE/PL), and UV−vis measurements have been performed via automated Philips X'Pert X-ray diffractometer, Oxford 7538, Thermo Scientific K Alpha X-ray spectrometer, Bruker-Vertex 70, FESEM TESCAN MIRA3 (15 keV), FEI Talos F200S, Technai G2 F30 with a high-sensitivity HAADF-STEM detector, DriveAFM (Nanosurf), Cary Eclipse, and Cary 300 Bio Instruments, respectively. Luminance, EQE, and EL data were obtained inside an integrating sphere coupled with a Hamamatsu PMA-12 photonic multichannel analyzer and a Keithley 2400 source meter.

RESULTS AND DISCUSSION

Structural Analyses. *FESEM and HAADF-STEM Analysis.* Figure 1A−E shows the FESEM images of the samples prepared at various reaction times of 1, 2, 3, 4, and 6 h. Particularly, the formation of NWs is confirmed via the progress in reaction time. The NW-shaped inorganic semiconductors are generally formed through two different mechanisms of surfactant-assisted seeded growth and oriented attachment.[27] Based on the images obtained from FESEM, the growth mechanism follows the initial nucleation and Ostwald ripening of nanoparticles within the first hour of hydrothermal reaction, followed by their oriented attachment in the form of NW shape.[28] The HAADF-STEM image in Figure 1F also supports the formation of NW-shaped nanocomposites.

TEM Analysis. Figure 1G,H shows the direct images taken from hydrothermally prepared samples at 4 h of reaction. As shown, MSO particles are in a relatively long NW shape with an average length of 70 ± 7 nm and an average width of around 5 ± 0.3 nm. The NW shape of the present samples supports our assertion of their capability to promote the optoelectronic performances of a QLED. An interesting thing about this result is, unlike almost all the other reports dealing with nanosheets, nanoplates, monolayers, and QDs, the present work suggests a very simple route with inexpensive precursors and instruments to provide high-quality NWs of MSO composites for feeding all branches related to optoelectronics.

EDX Analysis. To evaluate if the prepared NWs are composed of Mo, S, and O elements, EDX analyses were performed using HAADF-STEM and SEM, confirming the presence of all expected elements (Figures 1I and 2A, respectively). Signals related to these elements are clear, while those of Mo and S overlap.

XRD Analysis. The crystallinity of a typical MSO sample was evaluated by XRD measurements. As can be seen in Figure 2B, the pattern is quite broad, implying the dominance of the quantum size regime in the prepared NWs. It is also a multipeak pattern that further proves the presence of both MoS_2 and MoO_3 crystalline phases when we compare it with the standard XRD peaks of MoS_2 and MoO_3 hexagonal bulk

https://doi.org/10.1021/acsaelm.2c00485
ACS Appl. Electron. Mater. 2022, 4, 3849−3859

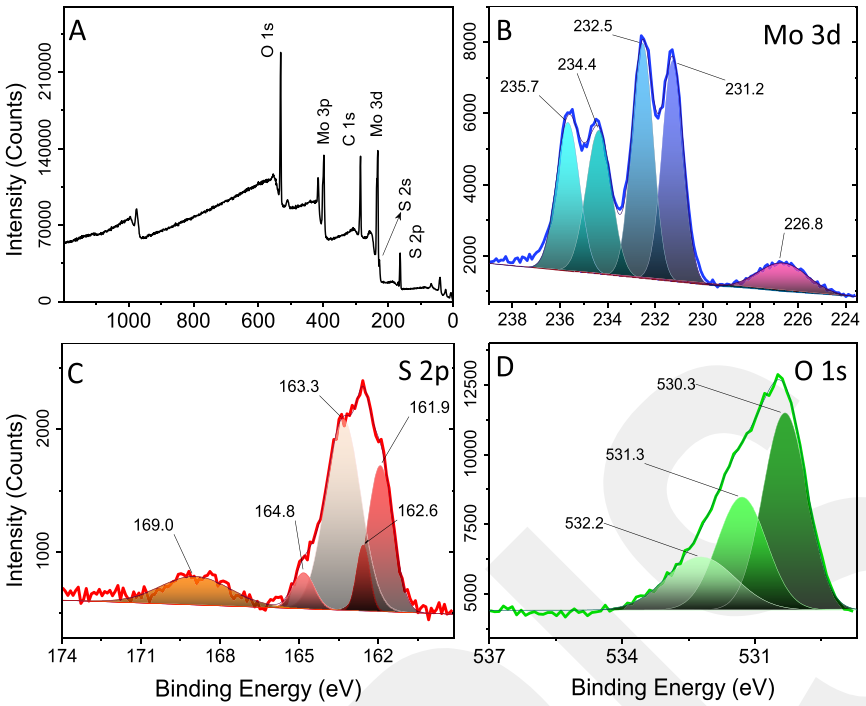

Figure 3. (A) XPS profile and (B–D) high-resolution XPS results for each element in the MSO NWs prepared at the temperature of 185 °C, concentration of 9.2 mM, solution pH of 3.7, and Mo/NAC/TU molar ratio of 1:2.4:2.

structures (bottom and top of the plot, respectively). Such observation has been reported elsewhere.[29,30]

FT-IR Spectroscopy. As we have used NAC in this synthesis, the situation of functional groups was analyzed by FT-IR spectroscopy. The bands located around 3473 and 1620 cm^{-1} are related to the O–H stretching and bending modes, respectively, while the vibrational signals that appeared at 3138 cm^{-1} belong to the N–H vibration groups of possible absorbed water. The weak peaks located around 2800 cm^{-1} are due to the symmetric and asymmetric vibrations of C–H groups. Thiols like NAC are known for their S–H-related sharp peak at around 2540 cm^{-1}.[31] However, it disappeared in the FT-IR spectrum of MSO nanocomposites. This indicated that S–H bonds deprotonated and S^- ions make complexes with Mo cations located at the surface of the nanocomposites. This may lead to the formation of nonstoichiometric states, as well. The intense peak at 1400 cm^{-1} originated from the C=O bonds. These deconvoluted peaks at around 900 cm^{-1} are associated with the M=O functional groups, while an intense band at 653 cm^{-1} is a characteristic peak of the Mo–O bond showing the possibility of formation of molybdenum oxide compounds. Finally, the relatively weak peak observed at 461 cm^{-1} is also assigned to the vibrational modes in Mo–S groups.[30] These results support the effective contribution of the NAC ligand in reaching high-quality nanocomposites.

XPS Analysis. Besides EDX analysis, XPS measurement was used to precisely find out the elements involved in the NWs and their chemical states (Figure 3). It demonstrated the presence of Mo, S, and O. As can be seen in high-resolution plots (Figure 3B–D), the Mo 3d region shows a multipeak pattern in which the ones located at 231.2 and 234.4 eV are attributed to the $3d_{5/2}$ and $3d_{3/2}$ binding energies of Mo(IV) in MoS_2, respectively. On the other hand, two intense signals at 232.5 and 235.7 eV are related to $3d_{5/2}$ and $3d_{3/2}$ of Mo(VI) in MoO_3,[32] respectively. The interesting point is that, almost in all reports related to MoS_2 or MoO_3, there are only two peaks.[32,33] However, in the present study, each one of the Mo-related peaks was deconvoluted into two peaks, indicating the presence of two types of Mo ions with different valence states. These observations confirm the formation of MSO composites.[19,34] It is worthy to note that generally in the MoS_2-included QDs, nanoflakes/sheets, and even bulks, the Mo^{4+}-related signals are located at around 229 and 232–233 eV.[35,36] These are a little bit different from the results presented here which can be assigned to the distinct NW morphology in the present MoS_2@MoO_3 composites. There is also a minor broad signal around 226.8 eV which is related to the S 2s energy levels. Figure 3C also shows that sulfur-related signals can be fitted to various well-resolved peaks. In this regard, peaks located at 161.9 and 162.6 eV are assigned to the $2p_{3/2}$ and $2p_{1/2}$ orbitals of S^{2-} (sulfur with −2 oxidation state), whereas XPS signals located at the binding energies of 163.3 and 164.8 eV are considered for bridging S_2^{2-}, respectively. This also supports the formation of some nonstoichiometric Mo_xS_y phases.[37,38] Besides, the one at 169.0 eV is due to the S–O bonds in sulfate groups. By analyzing the peak intensities, the atomic ratio of Mo/S/O was around 1:1.5:3.4, which is not in complete accordance with the theoretical stoichiometries. This further implied the formation of the composition of MSO in the presence of possible nonstoichiometry species. Finally, the 1s state of O is deconvoluted into three peaks, related to C=O and Mo–O bonds (530.3 eV), C–O–C signals (531.3), and C–OH signals (532.2). It is worthwhile mentioning that the high-resolution XPS results for C (data have not been included here) confirmed the presence of COOH functional groups at 288.5 eV, further supporting the role of the carboxylic groups of NAC. All the structural analyses mentioned above strongly support the formation of MSO composite NWs.

Optical Analyses. Besides the structural analyses, which were carried out to show the composition and morphology of

https://doi.org/10.1021/acsaelm.2c00485
ACS Appl. Electron. Mater. 2022, 4, 3849–3859

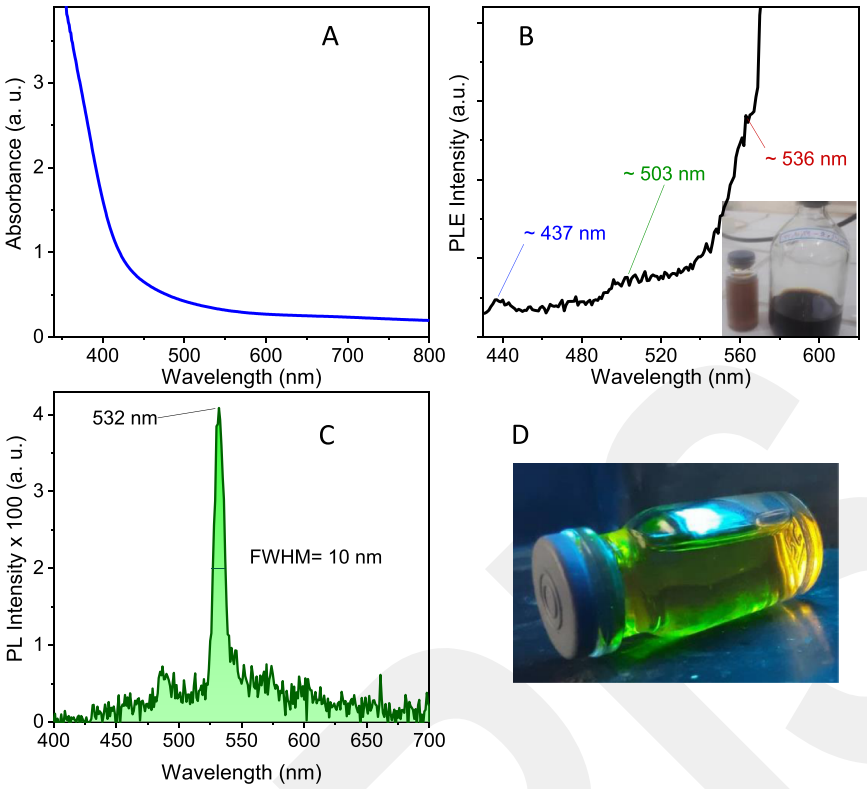

Figure 4. (A) UV−vis, (B) PLE (λ_{emi} = 600 nm; inset shows a digital photo of the as-prepared sample and its dilution), and (C) PL (λ_{exc} = 210 nm, a digital image of the as-prepared MSO NWs under UV irradiation) spectra of as-prepared MSO nanocomposites at the reaction temperature of 185 °C, solution concentration of 9.2 mM, solution pH of 3.7, and Mo/NAC/TU molar ratios of 1:2.4:2. (D) Corresponding digital image of the as-prepared MSO NWs under UV irradiation.

the prepared samples, a set of optical analyses were also performed, supporting the semiconducting nature of these nanocomposites. The reaction parameters are always of great importance in the solution-based colloidal synthesis approach. The key parameters determining the optical properties of such transition-metal trioxides or dichalcogenides are their shape and size. For example, the absorption edge for pure MoS_2 nanosheets is located at a wavelength range of 500−610 nm,[8,34] while hierarchical microspheres of PEGylated MoS_2 nanosheets and MoO_3 nanorods show absorption at short wavelengths.[30] Besides, the UV−vis absorption edge reported for blue-emissive MoS_2 QDs is also located at shorter wavelengths below 350 nm.[39,40] For the present MSO nanocomposite, various experimental parameters have been checked. Particularly, it was found that reaching the ultra-narrow emission in the green region is strongly dependent on the experimental conditions.

UV-vis. The UV−vis absorption spectra of the as-prepared samples at different experimental conditions have been recorded and shown in Figure S1. Regardless of the chosen experimental conditions, in all cases, there is a broad absorption onset and absorption tail with the lack of a strict excitonic peak. This confirmed the formation of the composition of two structures. As a general trend, the temperature of the thermal process is always an important factor governing the adequate energy for the growth of colloidal nanomaterials. Figure S1A shows that with the increase in the reaction temperature (from 140 to 185 °C), the amount of absorption goes up. On the other hand, there is an obvious red shift from 410 to 503 nm with an increase in the reaction temperature, implying the facilitated growth of nanocomposites. However, there are still controversies regarding the band gap type of such transition-metal dichalcogenides, whether they are in direct or indirect band gap mode.[41] Indeed, it depends on their lattice structure and dimension.[42] Using the Tauc relation,[43] the band gap energies for both the cases of direct and indirect modes were estimated. The direct band gap energies were 2.3, 3.15, and 3.35 eV, while the indirect band gaps were 2, 2.55, and 3.15 eV, at 185, 165, and 145 °C reaction temperatures, respectively. There is a decrease in band gap on increasing the reaction temperature. However, they are still larger than the band gap energy in the bulk structures of MoS_2 and MoO_3. Nonetheless, it should be mentioned that as the prepared samples are in nanocomposite form with some sort of nonstoichiometric phases (based on XPS results), it is not possible to provide a strict conclusion. As can be observed, the absorbance is too high at all wavelengths for the nanocomposites prepared at 185 °C (which was selected for further optimization). Therefore, the concentration of the initial solution was changed by changing the amounts of precursors used, at a fixed solution volume of 40 mL. In this regard, considering the hypothesis that all Mo precursors contribute to the reaction, the concentrations of the final product are 18.5, 9.2, and 4.6 mM. Figure S1B shows the results. As can be seen, there is a significant decrease in absorbance with a decrease in concentration, as well as a blue shift in the absorption region. The pH of the precursor solution is always an important parameter for reaching high-quality aqueous-soluble nanomaterials[44] (Figure S1C). The pH of the precursor solution was itself 3.7, which was adjusted to 8, 5.5, and 2, using NaOH or HCl. It was observed that with an increase in solution pH, the absorption spectrum shifts

https://doi.org/10.1021/acsaelm.2c00485
ACS Appl. Electron. Mater. 2022, 4, 3849−3859

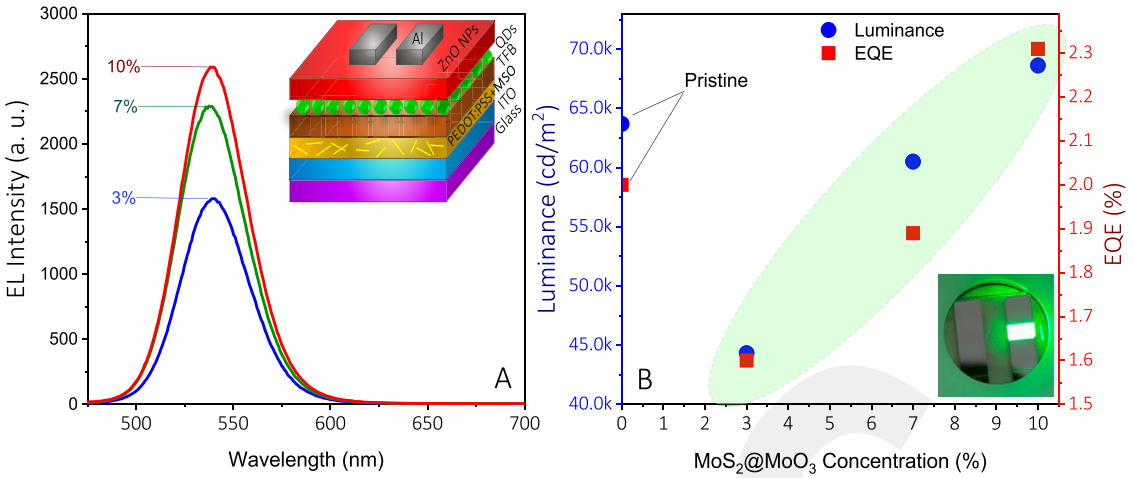

Figure 5. A) Electroluminescence spectra of QLEDs fabricated at different concentrations of MSO NWs. (B) Luminance and EQE values recorded for QLEDs fabricated at different concentrations of MSO NWs. Insets show a device structure and a digital image of fabricated green-emitting QLED.

remarkably toward shorter wavelengths as reported elsewhere.[34] This can be assigned to the wider band gap of MoO_3 compared to MoS_2. Indeed, nanocomposites prepared at higher pH values (with OH-rich solution) have wider band gap energies because the percentage of oxidized molybdenum is more. Hence, one can control the ratio of S-to-O in such composites by controlling the solution pH. Another important parameter is the molar ratio of the main precursors used for the reaction. The effect of the amount of Mo used on the UV−vis absorption spectrum of the prepared nanocomposites has been shown in Figure S1D. It shows that with an increase in the Mo precursor amount, the absorption edge experiences a red shift from 425 to 552 nm. Again, this can be attributed to the easier formation of MoS_2, which has a much smaller band gap than that of MoO_3. As mentioned earlier, and as demonstrated in the FT-IR spectrum, NAC molecules can play the role of the sulfur precursor as well. Figure S1E confirms that upon an increase in the NAC amount, there is a red shift in the absorption edge, indicating the contribution of more sulfur ions to the structure of the composite and subsequent easier formation of MoS_2 with a small band gap energy. The last precursor optimized was TU which is the main sulfur precursor. As Figure S1F shows, a similar trend was obtained here in which an increase in the sulfur precursor leads to a general red shift in the absorption spectrum. As confirmed in the FESEM images of MSO nanocomposites (Figure 1A−E), the reaction time is a very important factor governing the formation of the NW-shaped nanocomposites. However, the absorption spectrum can also provide a clue toward the growth mechanism of inorganic semiconductor NWs. Figure S1G reveals that upon an increase in the reaction time from 2 to 6 h, there is a red shift in the absorption edge as well as an increase in the absorbance, which somehow imply the dominance of the oriented attachment mechanism in these NWs.[27] The UV−vis absorption of the final sample with the best emission properties has been plotted in Figure 4A. Finally, Figure 4B shows the PL excitation (PLE) spectrum of a typical MSO nanocomposite sample,[45] along with the digital image of the as-prepared sample and diluted one. The color of the solution is the same as what has been reported elsewhere.[39,46]

Photoluminescence. While MoS_2 in the bulk form has no PL signal, there is a strong emission with a small full width in the present study. Splendiani et al., mentioned that while going down toward monolayers in nanoplate-shaped MoS_2, the Raman signals decrease due to the reduced amount of material, while the PL signals get bold.[42] In the following, the considerable effect of each experimental variable on the PL emission characteristics (under excitation at 210 nm) of the as-prepared MSO NWs is demonstrated. First, the precursors were dissolved in DI water in an ice bath because there was no PL emission signal for samples prepared via stirring at room temperature. The PL emission plot in Figure 4C shows a relatively strange plot with a noise-shaped peak, with strong intensity at 532 nm and ultra-narrow full width at half-maximum (fwhm) of 10 nm. Among the selected temperatures, samples prepared at 185 °C show a strong emission at 533 nm (Figure S2A). Samples prepared at different reaction temperatures looked too concentrated (nominal concentration of [Mo] = 18.5 mM). Hence, the next parameter was the concentration of precursors used. As mentioned earlier, without a change in the solvent volume, the amounts of all materials changed with the same molar ratio. Figure S2B proves a remarkable enhancement in emission intensity (about 3 times increase), with a decrease in concentration from 18.5 to 9.2 mM, while the FWHM remained constant. Solution pH is also a factor governing the growth and composition of the final product, in a polar medium. As can be seen in Figure S2C, the best result emerged for pH = 3.7. By evaluating the amounts of precursors (Figure S2D−F), it was demonstrated that the best PL emission results are achieved for the Mo/NAC/TU molar ratio of 1:2.4:2. As the last experimental parameter, the reaction time was checked for MSO NWs prepared at the temperature of 185 °C, the concentration of 9.2 mM, solution pH of 3.7, and Mo/NAC:TU molar ratio of 1:2.4:2. In this situation, the best PL emission results were obtained for 4 h of heating (Figure S2G). To visually support the intense and narrow PL emission signal, the as-prepared finally optimized sample was subjected to irradiation of a 6 W UV lamp at 254 nm. As can be seen in Figure 4D, there is a pure green emission. The green and pure PL emission recorded in this study is quite different from almost all the already published reports on similar colloidal nanomaterials.[39,47,48] Therefore, the optical data observed here still need more evaluation to be authenticated.

https://doi.org/10.1021/acsaelm.2c00485
ACS Appl. Electron. Mater. 2022, 4, 3849−3859

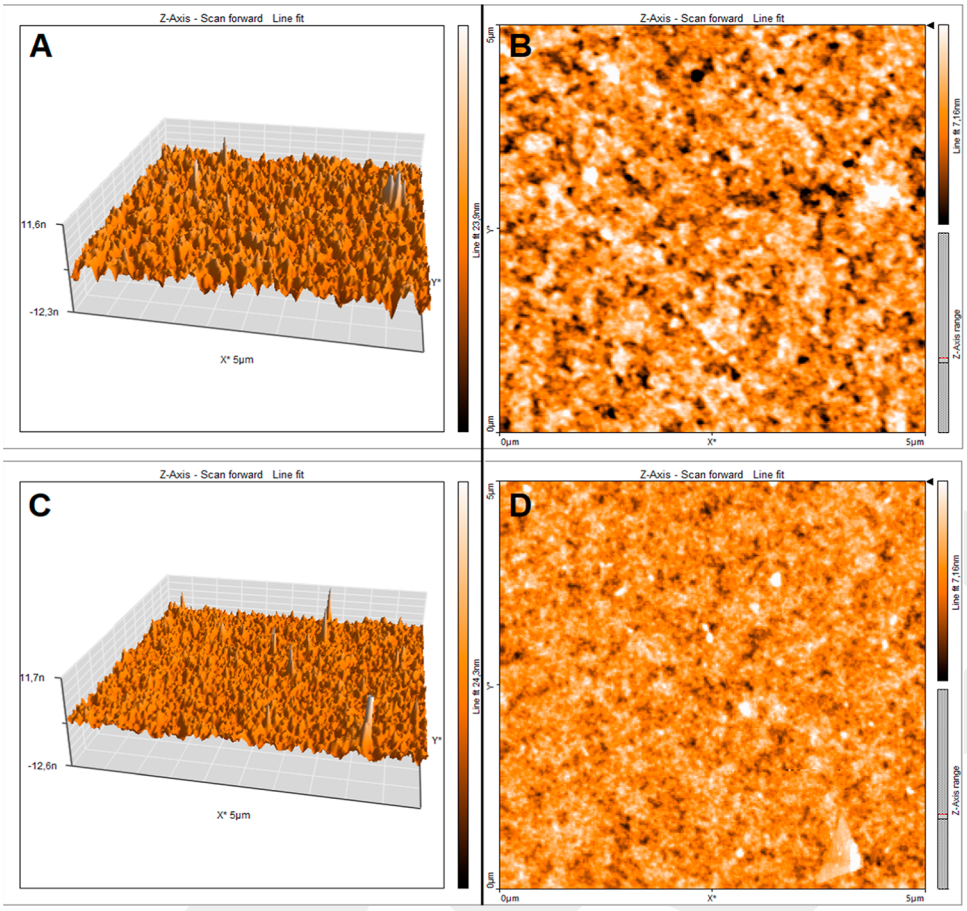

Figure 6. Two- and three- dimensional AFM images of PEDOT:PSS layer (A,B) without MSO NWs and (C,D) with 10% MSO NWs.

QLED Results. As a proof-of-concept demonstration of the practical merits of the prepared MSO NWs in enhancing the performance of QLEDs, they were blended into a PEDOT/PSS solution and spin-coated as HIL. Fine powders of MSO NWs were dissolved in DI water (1 mg/mL) and mixed with the PEDOT/PSS solution in different volume ratios of 0, 3, 7, and 10%, instead of the solid fraction ratio such as that in ref 18. The device structure is typically designed as anode/HIL/HTL/emitter layer (EML)/electron transport layer (ETL)/cathode in which all the layers were spin-coated except the anode and cathode. The EML used in the presented QLED prototype was fabricated using green-emissive CdSe/ZnS QDs, with the PL signal at 529 nm, FWHM of 33.7 nm, and PLQY of around 80% (Figure S3). The inset of Figure 5A shows a schematic of the device architecture and a digital photograph of the fabricated QLEDs. The electroluminescence (EL) spectra of green QLEDs fabricated with different amounts of MSO have been recorded at the voltage range of 0.7−20 V (Figure 5A,B). As can be seen, the EL peak is located at around 540 nm, with FWHM as narrow as 32 nm. As an overall trend, with the addition of MSO NWs, EL intensity increased remarkably. Nonetheless, there is a decrease in EL intensity, luminance, and EQE of QLED, compared to the pristine PEDOT:PSS, upon the addition of 3% of MSO NWs. This can be either due to the change in the surface thickness/roughness of the deposited HIL or an increase in the energy barrier for hole injection upon the initial addition of MSO NWs.[18] However, with a further increase in the concentration of MSO to 7%, there is a dramatic enhancement in the QLED optoelectronic features. Indeed, the luminance and EQE increased from 44,330 cd.m^{-2} and 1.6% to 60,510 cd.m^{-2} and 1.9%, respectively. Therefore, with a further increase in the content of MSO NWs in PEDOT:PSS to 7% and then 10%, luminance (68,630 cd.m^{-2}) and EQE (2.31%) enhanced remarkably, which are higher than that of pristine PEDOT:PSS (63,690 cd.m^{-2} and 2%). These results confirmed the overall positive role of MSO NWs in promoting the optoelectronic properties of a QLED. The influence of the increasing content of MSO in PEDOT:PSS on the optoelectronic features of QLEDs has been highlighted in Figure 5B.

It seems that there is a combination of two positive effects for the addition of MSO NWs. On one side, the presence of MSO decreases both the surface and line roughnesses, as shown from the AFM measurements of the coated substrates (Figure 6). Data revealed that the surface and line roughnesses reduce from 1.50 and 1.55 nm in MSO-free PEDOT: PSS layer to 1.30 and 0.84 nm for PEDOT:PSS layer with 10% MSO, respectively. On the other hand, the intrinsic electronic properties of the NW-shaped semiconductors of MSO nanocomposites can improve the carrier transport (Figure S4). Indeed, concerning the luminance and EQE peaks, the peak values of the current efficiency in various applied voltages showed an enhanced result in the presence of 10% MSO NWs blended with PEDOT/PSS. Kim et al.[13] demonstrated that incorporating 0.2 vol % MoO_3 into PEDOT: PSS causes around 0.15 eV decrease in the conduction band maximum. Nonetheless, we added a substantial amount of MSO compared to their work, so it can be postulated that the

https://doi.org/10.1021/acsaelm.2c00485
ACS Appl. Electron. Mater. 2022, 4, 3849−3859

work function of PEDOT: PSS was enhanced. To summarize these observations, the deep-lying conduction band of MSO introduces a barrier to carrier transport. However, the p-doping effect of MSO outweighs the initial detrimental effects as the concentration increases from 3 to 10%. Increased carrier concentration facilitates more balanced carrier recombination, which is reflected as an enhancement of luminance and EQE in the current QLED devices.[13] Also, AFM results show that NW-MSO addition to PEDOT: PSS lowers the surface roughness reasonably. Therefore, a more uniform thin-film formation would lead to the facilitated hole injection from PEDOT:PSS to the TFB layer.

Finally, using an inorganic hole injection layer[49,50] or even an all-inorganic transport layer[51,52] is an effective way to improve the operating lifetime of QLEDs, which has been already demonstrated. To reference this important aspect of the fabricated QLED, HIL coating was done by preparing MSO-PEDOT: PSS mixtures at the ratios of 0 and 10% by volume. The lifetime measurements of the devices were completed with the luminance vs. time graph at the same current densities (Figure S5). It was observed that upon 5 h of QLED operation, the luminance of the MSO-free device decreased to 19.17% of the initial value, while the device with MSO added remained more stable and decreased to 24.97% of the initial value. As a result, it was observed that the addition of MSO created a difference of 30.26% between the final values during 5 h operation under a constant current density, confirming its positive effect on device stability.

CONCLUSIONS

In summary, NWs of MSO composites were prepared via a facile hydrothermal method, at 185 °C for 4 h reaction. The optimized composites were long NWs with an average length of 70 nm which showed a green color PL signal with an ultra-small fwhm. XPS analyses confirmed the presence of Mo ions in various valence states, supporting the formation of MSO nanocomposites. Then, to support the idea of practical advantages of these NWs for optoelectronic devices, different volumes of MSO NWs were added into the PEDOT:PSS solution and deposited as a HIL in a well-designed QLED. The recorded data confirmed that upon an increase in the content of MSO NWs in PEDOT:PSS from 3 to 10%, the luminance and EQE improves from 44,330 cd.m^{-2} and 1.6% to 68,630 cd.m^{-2} and 2.3%, respectively. The electrical and AFM morphological measurements confirmed that both the enhanced charge transport and smoother surface roughness are responsible for such promotion in the device performance and durability. The simplicity and cost-effective features of the synthesis method along with outstanding favorable morphology demonstrated the ability to improve the QLED performance and mark them as a potentially universal material for optoelectronics.

ASSOCIATED CONTENT

Supporting Information

The Supporting Information is available free of charge at https://pubs.acs.org/doi/10.1021/acsaelm.2c00485.

UV−vis spectra, PLE, and PL spectra of the MSO nanocomposites under different reaction conditions; UV−vis/PL spectra of the CdSe/ZnS QDs; current efficiency vs. voltage plots; and stability analysis of the QLEDs (PDF)

AUTHOR INFORMATION

Corresponding Authors

Ehsan Soheyli − *Department of Electrical-Electronics Engineering, Abdullah Gul University, Kayseri 38080, Turkey; Department of Physics, Faculty of Science, Ilam University, 65315-516 Ilam, Iran*; Email: ehsan.soheyli@agu.edu.tr

Reza Sahraei − *Department of Chemistry, Faculty of Science, Ilam University, 65315-516 Ilam, Iran*; orcid.org/0000-0001-7104-2126; Email: r.sahraei@ilam.ac.ir

Evren Mutlugun − *Department of Electrical-Electronics Engineering, Abdullah Gul University, Kayseri 38080, Turkey; UNAM-Institute of Materials Science and Nanotechnology, Bilkent University, Ankara 06800, Turkey*; orcid.org/0000-0003-3715-5594; Email: evren.mutlugun@agu.edu.tr

Authors

Nasim Bastami − *Department of Chemistry, Faculty of Science, Ilam University, 65315-516 Ilam, Iran*

Ayşenur Arslan − *Department of Electrical-Electronics Engineering, Abdullah Gul University, Kayseri 38080, Turkey*

Ahmet Faruk Yazici − *Department of Nanotechnology Engineering, Abdullah Gul University, Kayseri 38080, Turkey*

Complete contact information is available at: https://pubs.acs.org/10.1021/acsaelm.2c00485

Author Contributions

N.B.: Investigation, formal analysis, and visualization (MSO NWs). E.S.: Conceptualization, investigation, data curation, methodology, validation, writing−−original draft, writing−−review, and editing. A.A.: Investigation, formal analysis, visualization (device fabrication). R.S.: Conceptualization, funding acquisition, project administration, resources, writing−−review and editing. A.F.Y.: Formal analysis (synthesis of QDs). E.M.: Conceptualization, funding acquisition, project administration, resources, writing−−review and editing.

Notes

The authors declare no competing financial interest.

REFERENCES

(1) Litvin, A. P.; Martynenko, I. V.; Purcell-Milton, F.; Baranov, A. V.; Fedorov, A. V.; Gun'ko, Y. K. Colloidal Quantum Dots for Optoelectronics. *J. Mater. Chem. A* **2017**, *5*, 13252−13275.

(2) Liu, B.; Altintas, Y.; Wang, L.; Shendre, S.; Sharma, M.; Sun, H.; Mutlugun, E.; Demir, H. V. Record High External Quantum Efficiency of 19.2% Achieved in Light-Emitting Diodes of Colloidal Quantum Wells Enabled by Hot-Injection Shell Growth. *Adv. Mater.* **2019**, *32*, 9567.

(3) Wang, F.; Wang, Z.; Zhu, X.; Bai, Y.; Yang, Y.; Hu, S.; Liu, Y.; You, B.; Wang, J.; Li, Y.; Tan, Z. A. Highly Efficient and Super Stable Full-Color Quantum Dots Light-Emitting Diodes with Solution-Processed All-Inorganic Charge Transport Layers. *Small* **2021**, *17*, 2007363.

(4) Qi, D.; Xie, L.; Yang, M.; Meng, X.; Yi, Y.-Q.-Q.; Hao, Y.; Su, W.; Xu, L.; Gai, Y.; Cui, Z. Finely Controlled Synthesis of $Zn_{1-X}Mg_xO$ Nanoparticles with Uniform Size Distribution Used as Electron Transport Materials for Red QLEDs. *ACS Appl. Electron. Mater.* **2022**, *4*, 1875−1881.

(5) Reza, K. M.; Gurung, A.; Bahrami, B.; Mabrouk, S.; Elbohy, H.; Pathak, R.; Chen, K.; Chowdhury, A. H.; Rahman, M. T.; Letourneau, S.; Yang, H. C.; Saianand, G.; Elam, J. W.; Darling, S. B.; Qiao, Q. Tailored PEDOT:PSS Hole Transport Layer for Higher Performance in Perovskite Solar Cells: Enhancement of Electrical and Optical

Properties with Improved Morphology. *J. Energy Chem.* **2020**, *44*, 41−50.
(6) Khasim, S.; Pasha, A.; Lakshmi, M.; Chellasamy, P.; Kadarkarai, M.; Darwish, A. A. A.; Hamdalla, T. A.; Al-Ghamdi, S. A.; Alfadhli, S. Post Treated PEDOT-PSS Films with Excellent Conductivity and Optical Properties as Multifunctional Flexible Electrodes for Possible Optoelectronic and Energy Storage Applications. *Opt. Mater.* **2022**, *125*, 112109.
(7) Song, D.-H.; Song, S.-H.; Shen, T.-Z.; Lee, J.-S.; Park, W.-H.; Kim, S.-S.; Song, J.-K. Quantum Dot Light-Emitting Diodes Using a Graphene Oxide/PEDOT:PSS Bilayer as Hole Injection Layer. *RSC Adv.* **2017**, *7*, 43396−43402.
(8) Lagonegro, P.; Martella, C.; Squeo, B. M.; Carulli, F.; Scavia, G.; Lamperti, A.; Galeotti, F.; Dubertret, B.; Pasini, M.; Brovelli, S.; Molle, A.; Giovanella, U. Prolonged Lifetime in Nanocrystal Light-Emitting Diodes Incorporating MoS_2-Based Conjugated Polyelectrolyte Interfacial Layer as an Alternative to PEDOT:PSS. *ACS Appl. Electron. Mater.* **2020**, *2*, 1186−1192.
(9) Huang, X.; Bäuerle, R.; Scherz, F.; Tisserant, J.-N.; Kowalsky, W.; Lovrinčić, R.; Hernandez-Sosa, G. Improved Performance of Perovskite Light-Emitting Diodes with a NaCl Doped PEDOT:PSS Hole Transport Layer. *J. Mater. Chem. C* **2021**, *9*, 4344−4350.
(10) Wang, L.; Pan, J.; Qian, J.; Liu, C.; Zhang, W.; Akram, J.; Lei, W.; Chen, J. Performance Enhancement of All-Inorganic Quantum Dot Light-Emitting Diodes via Surface Modification of Nickel Oxide Nanoparticles Hole Transport Layer. *ACS Appl. Electron. Mater.* **2019**, *1*, 2096−2102.
(11) Ponomarev, E.; Pásztor, Á.; Waelchli, A.; Scarfato, A.; Ubrig, N.; Renner, C.; Morpurgo, A. F. Hole Transport in Exfoliated Monolayer MoS2. *ACS Nano* **2018**, *12*, 2669−2676.
(12) Dong, J.; Fang, W.; Yuan, H.; Xia, W.; Zeng, X.; Shangguan, W. Few-Layered MoS_2/ZnCdS/ZnS Heterostructures with an Enhanced Photocatalytic Hydrogen Evolution. *ACS Appl. Energy Mater.* **2022**, *5*, 4893−4902.
(13) Kim, D. B.; Yu, J. C.; Nam, Y. S.; Kim, D. W.; Jung, E. D.; Lee, S. Y.; Lee, S.; Park, J. H.; Lee, A.-Y.; Lee, B. R.; Di Nuzzo, D.; Friend, R. H.; Song, M. H. Improved Performance of Perovskite Light-Emitting Diodes Using a PEDOT:PSS and MoO3 Composite Layer. *J. Mater. Chem. C* **2016**, *4*, 8161−8165.
(14) Zhang, H.; Chen, S.; Sun, X. W. Efficient Red/Green/Blue Tandem Quantum-Dot Light-Emitting Diodes with External Quantum Efficiency Exceeding 21. *ACS Nano* **2018**, *12*, 697−704.
(15) Zheng, G.; Wang, T.; Lou, Q.; Shen, C.; Wu, M.; Sun, J.; Ji, W.; Zang, J.; Liu, K.; Dong, L.; Shan, C. Localized Excitonic Electroluminescence from Carbon Nanodots. *J. Phys. Chem. Lett.* **2022**, *13*, 1587−1595.
(16) Tan, Y.; Zhang, W.; Xiao, X.; Sun, J.; Ma, J.; Zhang, T.; Mei, G.; Wang, Z.; Zhao, F.; Wu, D.; Choy, W. C.; Sun, X. W.; Wang, K. Enhancing Hole Injection by Electric Dipoles for Efficient Blue InP QLEDs. *Appl. Phys. Lett.* **2021**, *119*, 221105.
(17) Pandey, P. K.; Ulla, H.; Satyanarayan, M. N.; Rawat, K.; Gaur, A.; Gawali, S.; Hassan, P. A.; Bohidar, H. B. Fluorescent MoS_2 Quantum Dot−DNA Nanocomposite Hydrogels for Organic Light-Emitting Diodes. *ACS Appl. Nano Mater.* **2020**, *3*, 1289−1297.
(18) Sorrentino, R.; Worsely, R.; Lagonegro, P.; Martella, C.; Alieva, A.; Scavia, G.; Galeotti, F.; Pasini, M.; Dubertret, B.; Brovelli, S.; Molle, A.; Casiraghi, C.; Giovanella, U. Hybrid MoS_2/PEDOT:PSS Transporting Layers for Interface Engineering of Nanoplatelet-Based Light-Emitting Diodes. *Dalton Trans.* **2021**, *50*, 9208−9214.
(19) Singh, S.; Deb, J.; Sarkar, U.; Sharma, S. MoS_2/MoO_3 Nanocomposite for Selective NH_3 Detection in a Humid Environment. *ACS Sustainable Chem. Eng.* **2021**, *9*, 7328−7340.
(20) Rehman, M. M.; Siddiqui, G. U.; Gul, J. Z.; Kim, S. W.; Lim, J. H.; Choi, K. H. Resistive Switching in All-Printed, Flexible and Hybrid MoS2-PVA Nanocomposite Based Memristive Device Fabricated by Reverse Offset. *Sci. Rep.* **2016**, *6*, 36195.
(21) Choi, G. J.; Van Le, Q.; Choi, K. S.; Kwon, K. C.; Jang, H. W.; Gwag, J. S.; Kim, S. Y. Polarized Light-Emitting Diodes Based on Patterned MoS2 Nanosheet Hole Transport Layer. *Adv. Mater.* **2017**, *29*, 1702598.
(22) Fanourakis, S. K.; Peña-Bahamonde, J.; Rodrigues, D. F. Inorganic Salts and Organic Matter Effects on Nanorod, Nanowire, and Nanoplate MoO3 Aggregation, Dissolution, and Photocatalysis. *Environ. Sci.: Nano* **2020**, *7*, 3794−3804.
(23) Guo, S.; Li, X.; Ren, X.; Yang, L.; Zhu, J.; Wei, B. Optical and Electrical Enhancement of Hydrogen Evolution by MoS_2@MoO_3 Core−Shell Nanowires with Designed Tunable Plasmon Resonance. *Adv. Funct. Mater.* **2018**, *28*, 1802567.
(24) Liu, H.; Chen, X.; Deng, L.; Ding, M.; Li, J.; He, X. Perpendicular Growth of Few-Layered MoS_2 Nanosheets on MoO3 Nanowires Fabricated by Direct Anion Exchange Reactions for High-Performance Lithium-Ion Batteries. *J. Mater. Chem. A* **2016**, *4*, 17764−17772.
(25) Altintas, Y.; Genc, S.; Talpur, M. Y.; Mutlugun, E. CdSe/ZnS Quantum Dot Films for High-Performance Flexible Lighting and Display Applications. *Nanotechnology* **2016**, *27*, 295604.
(26) Lee, K.-H.; Lee, J.-H.; Song, W.-S.; Ko, H.; Lee, C.; Lee, J.-H.; Yang, H. Highly Efficient, Color-Pure, Color-Stable Blue Quantum Dot Light-Emitting Devices. *ACS Nano* **2013**, *7*, 7295−7302.
(27) Tong, Y.; Bohn, B. J.; Bladt, E.; Wang, K.; Müller-Buschbaum, P.; Bals, S.; Urban, A. S.; Polavarapu, L.; Feldmann, J. From Precursor Powders to $CsPbX_3$ Perovskite Nanowires: One-Pot Synthesis, Growth Mechanism, and Oriented Self-Assembly. *Angew. Chem., Int. Ed.* **2017**, *56*, 13887−13892.
(28) Sahraei, R.; Mihandoost, A.; Nabiyouni, G.; Daneshfar, A.; Roushani, M.; Majles Ara, M. Room Temperature Synthesis and Characterization of Ultralong $Cd(OH)_2$ Nanowires: A Simple and Template-Free Chemical Route. *Appl.Phys.A: Mater.Sci.Process.* **2012**, *109*, 471−475.
(29) Joseph, N.; Bose, A. C. One-Pot Synthesis of MoO_3/MoS_2 Composite and Investigation on Its Electrochemical Charge Storage Properties. *AIP Conf. Proc.* **2019**, *2115*, 30551.
(30) Kumar, N.; George, B. P. A.; Abrahamse, H.; Parashar, V.; Ngila, J. C. Sustainable One-Step Synthesis of Hierarchical Microspheres of PEGylated MoS_2 Nanosheets and MoO3 Nanorods: Their Cytotoxicity towards Lung and Breast Cancer Cells. *Appl. Surf. Sci.* **2017**, *396*, 8−18.
(31) Soheyli, E.; Sahraei, R.; Nabiyouni, G. PH-Dependent Optical Properties of N-Acetyl-L-Cysteine-Capped ZnSe(S) Nanocrystals with Intense/Stable Emissions. *J. Nanopart. Res.* **2017**, *19*, 92−106.
(32) Liu, Y.; Feng, P.; Wang, Z.; Jiao, X.; Akhtar, F. Novel Fabrication and Enhanced Photocatalytic MB Degradation of Hierarchical Porous Monoliths of MoO_3 Nanoplates OPEN. *Sci. Rep.* **2017**, *7*, 1845.
(33) Xu, X.; Mo, L.; Li, W.; Li, Y.; Lei, B.; Zhang, X.; Zhuang, J.; Hu, C.; Liu, Y. Red, Green and Blue Aggregation-induced Emissive Carbon Dots. *Chin. Chem. Lett.* **2021**, *32*, 3927−3930.
(34) Lai, M. T. L.; Lee, K. M.; Yang, T. C. K.; Pan, G. T.; Lai, C. W.; Chen, C.-Y.; Johan, M. R.; Juan, J. C. The Improved Photocatalytic Activity of Highly Expanded MoS_2 under Visible Light Emitting Diodes. *Nanoscale Adv.* **2021**, *3*, 1106−1120.
(35) Li, B.; Jiang, L.; Li, X.; Ran, P.; Zuo, P.; Wang, A.; Qu, L.; Zhao, Y.; Cheng, Z.; Lu, Y. Preparation of Monolayer MoS_2 Quantum Dots Using Temporally Shaped Femtosecond Laser Ablation of Bulk MoS2 Targets in Water. *Sci. Rep.* **2017**, *7*, 11182.
(36) Kesavan, D.; Mariappan, V. K.; Pazhamalai, P.; Krishnamoorthy, K.; Kim, S.-J. Topochemically Synthesized MoS_2 Nanosheets: A High Performance Electrode for Wide-Temperature Tolerant Aqueous Supercapacitors. *J. Colloid Interface Sci.* **2021**, *584*, 714−722.
(37) Samaniego-Benitez, J. E.; Mendoza-Cruz, R.; Bazán-Díaz, L.; Garcia-Garcia, A.; Arellano-Jimenez, M. J.; Perez-Robles, J. F.; Plascencia-Villa, G.; Velázquez-Salazar, J. J.; Ortega, E.; Favela-Camacho, S. E.; José-Yacamán, M. Synthesis and Structural Characterization of MoS_2 Micropyramids. *J. Mater. Sci.* **2020**, *55*, 12203−12213.

https://doi.org/10.1021/acsaelm.2c00485
ACS Appl. Electron. Mater. 2022, 4, 3849−3859

(38) Liu, J.; Zhong, Y.; Li, X.; Ying, T.; Han, T.; Li, J. A Novel Rose-with-Thorn Ternary MoS_2@carbon@polyaniline Nanocomposite as a Rechargeable Magnesium Battery Cathode Displaying Stable Capacity and Low-Temperature Performance. *Nanoscale Adv.* **2021**, *3*, 5576−5580.
(39) Ren, X.; Pang, L.; Zhang, Y.; Ren, X.; Fan, H.; Liu, S. One-Step Hydrothermal Synthesis of Monolayer MoS_2 Quantum Dots for Highly Efficient Electrocatalytic Hydrogen Evolution. *J. Mater. Chem. A* **2015**, *3*, 10693−10697.
(40) Gu, W.; Yan, Y.; Zhang, C.; Ding, C.; Xian, Y. One-Step Synthesis of Water-Soluble MoS_2 Quantum Dots via a Hydrothermal Method as a Fluorescent Probe for Hyaluronidase Detection. *ACS Appl. Mater. Interfaces* **2016**, *8*, 11272−11279.
(41) Ellis, J. K.; Lucero, M. J.; Scuseria, G. E. The Indirect to Direct Band Gap Transition in Multilayered MoS2 as Predicted by Screened Hybrid Density Functional Theory. *Appl. Phys. Lett.* **2011**, *99*, 261908.
(42) Splendiani, A.; Sun, L.; Zhang, Y.; Li, T.; Kim, J.; Chim, C.-Y.; Galli, G.; Wang, F. Emerging Photoluminescence in Monolayer MoS_2. *Nano Lett.* **2010**, *10*, 1271−1275.
(43) Soheyli, E.; Sahraei, R.; Nabiyouni, G. Aqueous Based Synthesis of N-Acetyl-L-Cysteine Capped ZnSe Nanocrystals with Intense Blue Emission. *Opt. Mater.* **2016**, *60*, 564−570.
(44) Habibi Jetani, G.; Rahmani, M. B. Exploring the Effect of Hydrothermal Precursor PH on the Photosensitivity of 1T/2H−MoS_2 Nanosheets. *Opt. Mater.* **2022**, *124*, 111974.
(45) Yao, K.; Yan, A.; Kahn, S.; Suslu, A.; Liang, Y.; Barnard, E. S.; Tongay, S.; Zettl, A.; Borys, N. J.; Schuck, P. J. Optically Discriminating Carrier-Induced Quasiparticle Band Gap and Exciton Energy Renormalization in Monolayer MoS_2. *Phys. Rev. Lett.* **2017**, *119*, 087401.
(46) Yang, H.; Zhao, J.; Wu, C.; Ye, C.; Zou, D.; Wang, S. Facile Synthesis of Colloidal Stable MoS_2 Nanoparticles for Combined Tumor Therapy. *Chem. Eng. J.* **2018**, *351*, 548−558.
(47) Lu, G.-Z.; Wu, M.-J.; Lin, T.-N.; Chang, C.-Y.; Lin, W.-L.; Chen, Y. T.; Hou, C.-F.; Cheng, H.-J.; Lin, T.-Y.; Shen, J.-L.; Chen, Y. F. Electrically Pumped White-Light-Emitting Diodes Based on Histidine-Doped MoS_2 Quantum Dots. *Small* **2019**, *15*, 1901908.
(48) Santiago, S. R. M. S.; Wang, H.-J.; Chen, Y.-T.; Hsu, I.-J.; Wu, C.-B.; Hsu, K.-M.; Cheng, M.-C.; Lin, T.-N.; Feria, D. N.; Chou, W.-C.; Shen, J. L. Density-Dependent Carrier Recombination in MoS_2 Quantum Dots and Its Implications for Luminescence Sensing of Ammonium Hydroxide. *ACS Appl. Nano Mater.* **2020**, *3*, 11630−11637.
(49) Cao, F.; Wang, H.; Shen, P.; Li, X.; Zheng, Y.; Shang, Y.; Zhang, J.; Ning, Z.; Yang, X. High-Efficiency and Stable Quantum Dot Light-Emitting Diodes Enabled by a Solution-Processed Metal-Doped Nickel Oxide Hole Injection Interfacial Layer. *Adv. Funct. Mater.* **2017**, *27*, 1704278.
(50) Wu, Q.; Gong, X.; Zhao, D.; Zhao, Y.-B.; Cao, F.; Wang, H.; Wang, S.; Zhang, J.; Quintero-Bermudez, R.; Sargent, E. H.; et al. Efficient Tandem Quantum-Dot LEDs Enabled by An Inorganic Semiconductor-Metal-Dielectric Interconnecting Layer Stack. *Adv. Mater.* **2022**, *34*, 2108150.
(51) Yang, X.; Zhang, Z.-H.; Ding, T.; Wang, N.; Chen, G.; Dang, C.; Demir, H. V.; Sun, X. W. High-Efficiency All-Inorganic Full-Colour Quantum Dot Light-Emitting Diodes. *Nano Energy* **2018**, *46*, 229−233.
(52) Cao, F.; Wu, Q.; Sui, Y.; Wang, S.; Dou, Y.; Hua, W.; Kong, L.; Wang, L.; Zhang, J.; Jiang, T.; Yang, X. All-Inorganic Quantum Dot Light-Emitting Diodes with Suppressed Luminance Quenching Enabled by Chloride Passivated Tungsten Phosphate Hole Transport Layers. *Small* **2021**, *17*, 2100030.

https://doi.org/10.1021/acsaelm.2c00485
ACS Appl. Electron. Mater. 2022, 4, 3849−3859